Journal of Intensive Care

RESEARCH

Open Access

Mechanisms maintaining right ventricular contractility-to-pulmonary arterial elastance ratio in VA ECMO: a retrospective animal data analysis of RV–PA coupling

Kaspar F. Bachmann[1*], Per Werner Moller[2], Lukas Hunziker[3], Marco Maggiorini[4] and David Berger[1]

Abstract

Background To optimize right ventricular–pulmonary coupling during veno-arterial (VA) ECMO weaning, inotropes, vasopressors and/or vasodilators are used to change right ventricular (RV) function (contractility) and pulmonary artery (PA) elastance (afterload). RV–PA coupling is the ratio between right ventricular contractility and pulmonary vascular elastance and as such, is a measure of optimized crosstalk between ventricle and vasculature. Little is known about the physiology of RV–PA coupling during VA ECMO. This study describes adaptive mechanisms for maintaining RV–PA coupling resulting from changing pre- and afterload conditions in VA ECMO.

Methods In 13 pigs, extracorporeal flow was reduced from 4 to 1 L/min at baseline and increased afterload (pulmonary embolism and hypoxic vasoconstriction). Pressure and flow signals estimated right ventricular end-systolic elastance and pulmonary arterial elastance. Linear mixed-effect models estimated the association between conditions and elastance.

Results At no extracorporeal flow, end-systolic elastance increased from 0.83 [0.66 to 1.00] mmHg/mL at baseline by 0.44 [0.29 to 0.59] mmHg/mL with pulmonary embolism and by 1.36 [1.21 to 1.51] mmHg/mL with hypoxic pulmonary vasoconstriction ($p < 0.001$). Pulmonary arterial elastance increased from 0.39 [0.30 to 0.49] mmHg/mL at baseline by 0.36 [0.27 to 0.44] mmHg/mL with pulmonary embolism and by 0.75 [0.67 to 0.84] mmHg/mL with hypoxic pulmonary vasoconstriction ($p < 0.001$). Coupling remained unchanged (2.1 [1.8 to 2.3] mmHg/mL at baseline; −0.1 [−0.3 to 0.1] mmHg/mL increase with pulmonary embolism; −0.2 [−0.4 to 0.0] mmHg/mL with hypoxic pulmonary vasoconstriction, $p > 0.05$). Extracorporeal flow did not change coupling (0.0 [−0.0 to 0.1] per change of 1 L/min, $p > 0.05$). End-diastolic volume increased with decreasing extracorporeal flow (7.2 [6.6 to 7.8] ml change per 1 L/min, $p < 0.001$).

Conclusions The right ventricle dilates with increased preload and increases its contractility in response to afterload changes to maintain ventricular–arterial coupling during VA extracorporeal membrane oxygenation.

Keywords Extracorporeal membrane oxygenation, Right ventricular function, Ventriculo-arterial coupling, Homeometric adaption, Heterometric adaption

*Correspondence:
Kaspar F. Bachmann
kaspar.bachmann@insel.ch
Full list of author information is available at the end of the article

Introduction

Despite improved treatment options, including mechanical circulatory support, cardiogenic shock has a high mortality of up to 50%. The entry and exit strategies for mechanical support still show a substantial gap in knowledge and evidence [1, 2]. Randomized trials of extracorporeal membrane oxygenation (ECMO) in scenarios of cardiogenic shock provide negative results [3]. Still, veno-arterial (VA) ECMO remains a short-term salvage option for severe acute cardiac failure [1], including right heart failure. ECMO is complex and resource intense, accompanied by profound and often harmful alterations of circulatory physiology [2], such as increases in left ventricular afterload [4], extensive changes in gas exchange [5, 6], fibrosis of the lung [7], and activation of coagulation and inflammatory pathways [8]. To gain therapeutic benefit from such complex supportive treatment, a better understanding of the pathophysiology is needed [2].

Ventricular function is governed by contractility and afterload. Both parameters can be influenced by inotropes, vasopressors, or vasodilators. For a ventricle to work efficiently, contractility must match the afterload. This match is described by ventricular–arterial coupling—expressed as the ratio of ventricular elastance to arterial elastance in the pressure–volume loop of a cardiac beat. It is visually shown by the two lines intersecting at the end-systolic pressure (Figs. 1C and 2) [9]. Ventricular–arterial uncoupling occurs in various states of shock and heart failure and has prognostic value in left heart failure [10, 11], pulmonary hypertension and right heart failure [12, 13], including intensive care patients [14]. Little is known about ventricular–arterial coupling during veno-arterial ECMO. Because of its ability to provide a combined assessment of contractility and afterload and its importance for right ventricular energetics [12], right ventricular–pulmonary artery (RV–PA) coupling is an interesting therapeutic target for patients on ECMO and has prognostic relevance for successful weaning from VA EMCO [15]. Physiological data for RV–PA coupling under ECMO are lacking. This post hoc study [5, 16] describes RV–PA coupling during VA ECMO weaning trials and provides a physiological framework for mechanisms that determine RV–PA coupling during extracorporeal circulatory support.

Methods

After approval by the animal welfare committee of Bern (BE 111/18) and in accordance with the Swiss Ordinance on the Protection of Animals (TSchV 2008 455.1), 16 pigs (3 pilot animals, *Sus scrofa*, 6 males, 45.5 ± 3.3 kg) were centrally cannulated for VA ECMO [5, 16]. After sedation with ketamine (15 mg kg^{-1}), midazolam (0.5 mg kg^{-1}) and methadone (0.2 mg kg^{-1}) i.m., general anesthesia was induced with propofol to effect (1–4 mg kg^{-1} IV), and further maintained with continuous infusion of propofol (2–8 $mg*kg^{-1}*h^{-1}$) and fentanyl (5–10 $\mu g*kg^{-1}*h^{-1}$). More details on animal care, anesthesia, and experimental setup have been previously described [5, 16]. The report follows the applicable ARRIVE guidelines.

The protocol consisted of 1 L/min VA ECMO flow reductions (from 4 to 1 L/min) at baseline, followed by, in randomized order, experimental conditions simulating pulmonary embolization (PE) and hypoxic pulmonary vasoconstriction (HPV). HPV was achieved through left main bronchus intubation. PE was simulated by left pulmonary artery balloon inflation.

Tidal volume was 10 mL/kg for baseline and PE, and 6 mL/kg during HPV. Each condition was repeated with varying respiratory rates (10 and 15 for baseline and PE; 10 and 20 breaths per minute for HPV). Norepinephrine and epinephrine infusions were used to maintain adequate perfusion pressure.

Ultrasonic flow probes around the pulmonary artery and VA ECMO outlet measured pulmonary (Q_{Lung}) and VA ECMO (Q_{ECMO}) blood flows, respectively (Transonic, Ithaca, NY). Pressures were measured in the right and left atria, and pulmonary and left carotid arteries, with transducers leveled to the right atrium. Data were acquired using LabVIEW (National Instruments Corp., Austin, TX) with Soleasy (Alea Solutions, Zurich, Switzerland) and Hamilton Memory Box (Hamilton Medical, Bonaduz, Switzerland) at 100 Hz resolution.

We selected three respiratory cycles from each experimental condition (Fig. 1A). Datasets with missing data or artifacts were excluded after visual inspection. Stroke volumes (SV), pressure amplitudes, end-systolic pulmonary arterial and right atrial pressures were extracted from each cardiac cycle. Right ventricular maximum isovolumetric pressure (P_{isomax}), pulmonary arterial elastance (E_a), and end-systolic ventricular elastance (E_{es}) were determined (Fig. 1B, C) [9, 17]. We determined the inspiratory and expiratory cardiac cycle at the highest and lowest SV of any given respiratory cycle, respectively. Ventricular coupling was defined as E_{es}/E_a and ejection fraction (RVEF) as $E_{es}/(E_a+E_{es})$ [18]. End-diastolic volume was calculated from RVEF and SV, allowing for partial reconstruction of PV loops (Figs. 1C and 2). Stroke volume variation (SVV) was calculated as $(\text{amplitude}_{max} - \text{amplitude}_{min})$ divided by $(\text{amplitude}_{max}/2 + \text{amplitude}_{min}/2)$.

Impedance describes the total opposition of a vascular bed to the pulsatile flow. It is a more comprehensive measure than resistance, as it considers not only the static component of blood flow but also the pulsatile component [19, 20]. Pulmonary vascular impedance was calculated as the ratio between pressure and flow moduli

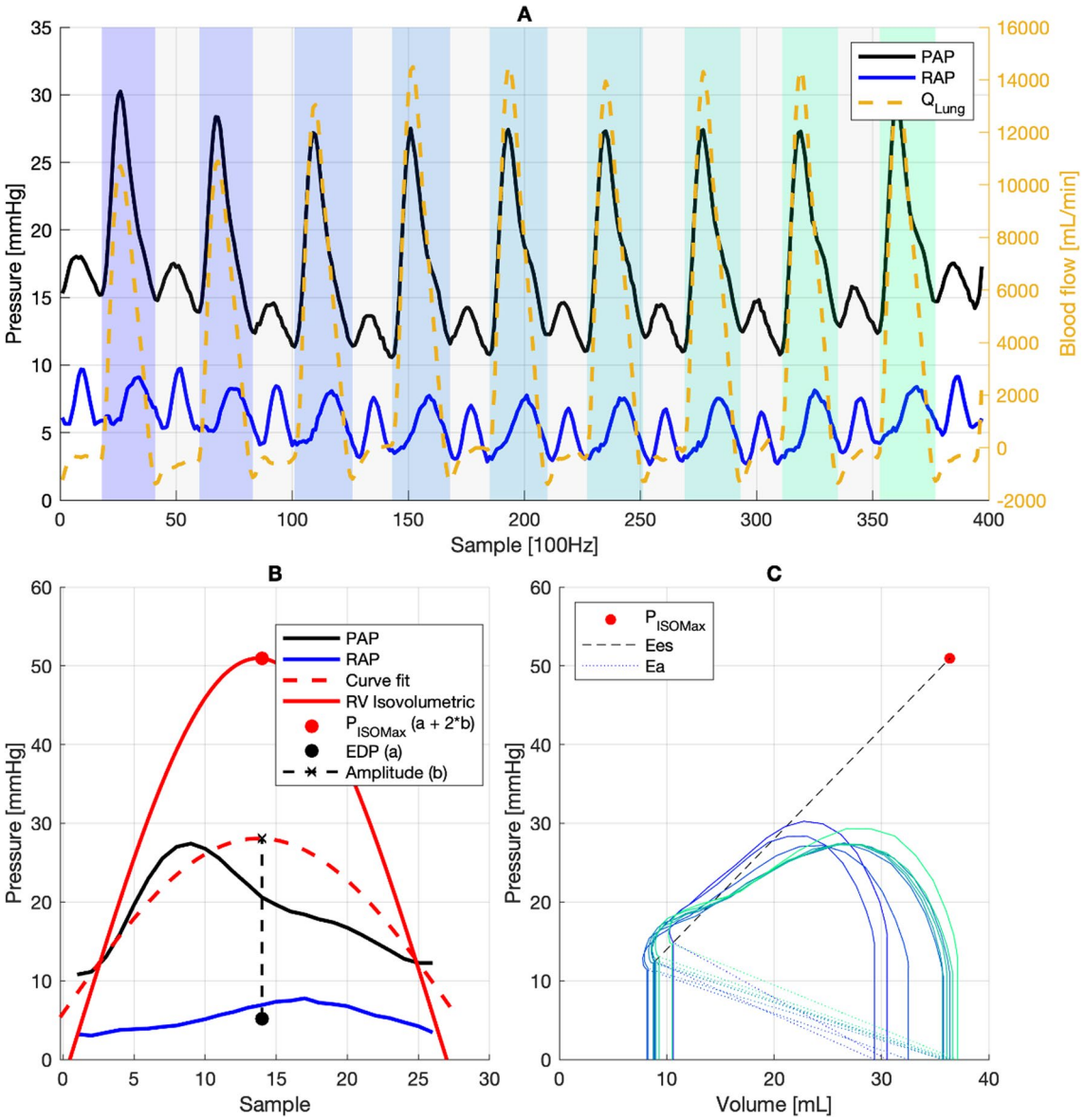

Fig. 1 Exemplary analysis of a full respiratory cycle (baseline condition, animal 2, Q_{ECMO} 829 mL/min). **A** Systoles (blue to green shaded areas) were identified using peak width analysis of the derivative of each pulmonary flow tracing, where the beginning of each peak (positive dQ/dt_{max}) defined the beginning of systoles. Beginnings of diastoles (uncolored areas) were identified through minimum pulmonary flow. Pressure and flow signals were aligned by determining the delay between dp/dt_{max} and dQ/dt_{max}. **B** A sine wave function $f(x) = a + b \times \sin(c \times x + d)$ was fitted through the systolic data points before dp/dt_{max} of the pressure rise and the end-systolic pulmonary arterial pressure. Coefficient a of the fit was forced to equal right ventricular end-diastolic pressure (RV_{EDP}), which was derived from the median right atrial pressure during the respective cardiac cycle. The curve fit was performed using a Levenberg–Marquardt algorithm [17]. P_{isomax} (maximum of isovolumetric right ventricular contraction) was then defined as $a + 2 \times b$ (**B**) [9, 17]. **C** Reconstruction of partial PV loops through calculation of end-diastolic volume, derived from $RVEF = E_{es}/(E_a + E_{es})$. E_{es} was extrapolated as the slope between end-systolic pressure and P_{isomax} from the cardiac cycle with the maximum stroke volume for a given respiratory cycle. As a load independent parameter, it was then assumed to be constant for all other cardiac cycles within a specific respiratory cycle [48, 49]. E_a was calculated as end-systolic PAP divided by stroke volume. E_{es}: Ventricular elastance. E_a: Arterial elastance

[19]. The input resistance was defined at 0 Hz (Z_0), and Z_c represented the average of impedance moduli between 2 and 15 Hz [19]. Total hydraulic power (W_T) was the integral of the instantaneous product of pressure times flow, and oscillatory hydraulic power (W_{Osc}) was W_T minus the product of mean pressure × mean flow [20]. Data are presented as mean with standard deviation or boxplots. Linear mixed-effects models were used to assess the impact

of Q_{ECMO} and experimental conditions on outcomes, with individual animals as random effects. Fixed effects (experimental condition and Q_{ECMO}) were entered as individual and interaction variables. r^2 represents goodness of fit. A p-value of < 0.05 was considered statistically significant. Data and statistical analysis were performed using MatLab (R2023a, MathWorks, Natick, MA, USA).

Results

Data from 13 animals were available. We extracted 1074 respiratory cycles from 358 conditions, of which 928 (86%) were included after visual exclusion of artifacts. All extracted datasets are available in Additional file 1.

Pressures and flows

Q_{ECMO} and ventilator settings followed the experimental protocol (Additional file 2: Table S1). At baseline, every 1 L/min reduction in Q_{ECMO} was associated with a 0.5 L/min increase in Q_{Lung} and approximately 0.5 mmHg increase in right and left atrial pressures (RAP and LAP, respectively). The increase in Q_{Lung} subsequently increased mean pulmonary artery pressure (mPAP) by approximately 1.8 mmHg for each 1 L/min decrease in Q_{ECMO}. Mean PAP almost doubled under HPV conditions, while SV and the resulting Q_{Lung} decreased compared to baseline. Of note, the regression model estimated not only a fixed increase in mPAP (+14.7 mmHg), but also estimated a steeper change associated with variations in Q_{ECMO} (−1.4 additional mmHg per increase of 1 L/min of Q_{ECMO}). RAP remained stable and LAP increased only slightly during HPV condition (+1.4 mmHg). The hemodynamic consequences introduced by PE were similar, but less pronounced as compared to HPV (Table 1, Additional file 2: Fig. S1). Support with norepinephrine (0.04 [0.03 to 0.08] µg/kg/min) and epinephrine (0.02 [0.00 to 0.03] µg/kg/min) was low-throughout experimental conditions (Additional file 2: Fig. S2).

Elastances

At baseline, end-systolic ventricular elastance (E_{es}) was approximately 0.8 mmHg/mL at zero Q_{ECMO} and was only marginally increased by higher Q_{ECMO} (0.07 mmHg/mL per change of 1 L/min). Expiratory PA elastance was 0.4 mmHg/mL in baseline (Fig. 3) and increased only slightly with increasing Q_{ECMO} (change of 0.04 mmHg/mL per change of 1 L/min, Table 2). Inspiratory arterial elastance (E_{aInsp}) remained unchanged from E_{aExp} at low Q_{ECMO} but increased markedly with increasing Q_{ECMO} (0.3 mmHg/mL, per change of 1 L/min) (Table 2, Figs. 2, 3).

In HPV and PE conditions, E_{es} increased (by 1.4 and 0.4 mmHg/mL, respectively), but, as seen at baseline, remained almost constant with varying Q_{ECMO}. In concordance with increasing E_{es}, E_{aExp} increased in HPV and PE conditions (by 0.8 and 0.4 mmHg/mL, respectively), without changing further with changing Q_{ECMO}. In contrast, E_{aInsp} showed substantial increases in HPV and PE conditions as compared to baseline. The increase was constant at HPV condition, without association to Q_{ECMO} (fixed increase of 0.9 mmHg/mL compared to baseline), while the increase at PE increased further with changing Q_{ECMO} (additional change of 0.7 mmHg/mL per increase of 1 L/min; Table 2, Figs. 2, 3).

Impedances

The pulmonary vascular impedance (Z_c) was estimated at 133 $dyn \times sec \times cm^{-5}$ for baseline condition at zero Q_{ECMO} and varied only minimally with Q_{ECMO} (13 $dyn \times sec \times cm^{-5}$ per increase of 1 L/min). Vascular impedance was not significantly altered during PE and HPV conditions (Table 3, Fig. 4). In contrast, the input resistance Z_0 increased significantly with increasing Q_{ECMO} (124 $dyn \times s \times cm^{-5}$ per change of 1 L/min from baseline, with impedance at zero Q_{ECMO} estimated to 268 $dyn \times s \times cm^{-5}$). HPV and PE conditions further increased Z_0 (fixed increases of 610 and 251 $dyn \times s \times cm^{-5}$, respectively), while the changes associated with Q_{ECMO} remained stable. The total hydraulic work (W_T) increased with decreasing Q_{ECMO} (change of −300 mW per increase of 1 L/min from an estimated 1609 mW at baseline and zero Q_{ECMO}). W_T was highest during HPV condition (additional fixed change of 888 mW, with a further decrease of −124 mW per change of 1 L/min). During PE condition, W_T increased significantly compared to baseline (increase of 251 mW, with further decrease of −81 mW per change of 1 L/min Q_{ECMO},). Similarly, W_{Osc} was highest during HPV condition (fixed increase of 273 mW

(See figure on next page.)

Fig. 2 Averaged PV loops (full lines) for each experimental condition. The left column are expiratory loops, the right column inspiratory loops. The vertical and horizontal error bars indicate 95% CI intervals for the respective parameter (end-systolic and end-diastolic volume on the abscissa, end-systolic pressure, early systolic pressure and P_{isomax} on the ordinate). The dashed lines indicate ventricular and pulmonary arterial elastance, respectively. Panels **A** and **B** show the averaged expiratory and inspiratory loops for baseline condition. Panel **C** and **D** show the averaged expiratory and inspiratory loops for hypoxic pulmonary vasoconstriction condition. Panel **E** and **F** show the averaged expiratory and inspiratory loops for pulmonary embolism condition

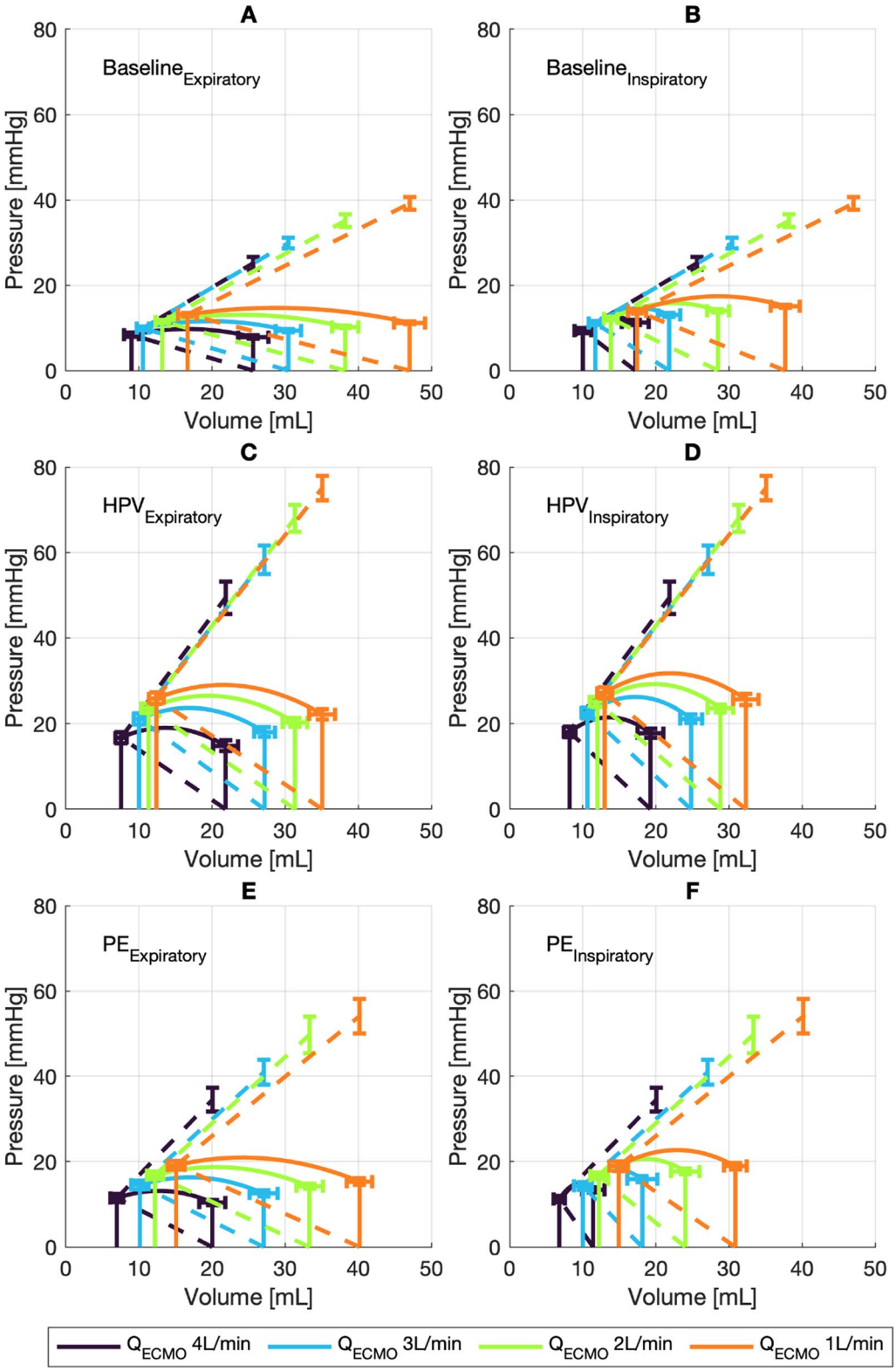

Fig. 2 (See legend on previous page.)

Table 1 Estimates from linear mixed-effect models predicting hemodynamic parameters

	RAP [mmHg]	LAP [mmHg]	Q_{Lung} [L/min]	mPAP [mmHg]
Intercept	6.1 [5.5 to 6.8]	6.4 [5.8 to 7.1]	3.1 [2.9 to 3.2]	17.8 [16.5 to 19.2]
HPV	−0.1 [−0.4 to 0.2]	1.4 [1.1 to 1.7]‡	−0.4 [−0.5 to −0.2]‡	14.7 [13.8 to 15.7]‡
PE	0.9 [0.6 to 1.2]‡	0.8 [0.5 to 1.1]‡	−0.2 [−0.3 to −0.1]‡	6.2 [5.3 to 7.2]‡
Q_{ECMO}	−0.5 [−0.6 to −0.4]‡	−0.6 [−0.7 to −0.6]‡	−0.5 [−0.5 to −0.5]‡	−1.8 [−2.0 to −1.6]‡
Q_{ECMO} × HPV	−0.4 [−0.5 to −0.2]‡	−0.1 [−0.2 to 0.1]	0.1 [0.1 to 0.2]‡	−1.4 [−1.7 to −1.0]‡
Q_{ECMO} × PE	−0.1 [−0.2 to −0.0]*	0.0 [−0.1 to 0.1]	0.0 [−0.0 to 0.1]	−0.8 [−1.2 to −0.5]‡
Adjusted r^2	0.76	0.75	0.76	0.84

Estimates from regression are shown with 95% CI. The intercept is the estimated value at 0 L/min Q_{ECMO} for baseline condition. HPV and PE estimates the change if the respective condition is present. Q_{ECMO} estimates the change per change of 1 L/min. Q_{ECMO} × HPV and Q_{ECMO} × PE estimates the additional change per change of 1 L/min of Q_{ECMO} during the respective condition. Q_{ECMO}: ECMO blood flow [L/min]. HPV: hypoxic pulmonary vasoconstriction. PE: pulmonary embolism. RAP: right atrial pressure. LAP: left atrial pressure. Q_{Lung}: pulmonary blood flow. mPAP: mean pulmonary arterial pressure. *$p < 0.05$. ‡$p < 0.001$

from an estimated baseline of 387 mW at zero Q_{ECMO},), clearly associated with changing Q_{ECMO} (−72 mW per increase of 1 L/min Q_{ECMO}, with an additional change of −40 mW per increase of 1 L/min). PE condition increased W_{Osc} by only 82 mW without further change with Q_{ECMO} (Table 3 and Fig. 4).

Coupling and stroke volume variations

The expiratory VA coupling was estimated to 2.1 at baseline and zero ECMO flow (Table 4, Figs. 2 and 5). The ratio remained stable at HPV and PE conditions, unaffected by changing Q_{ECMO}. Inspiratory VA coupling followed the changes described for E_{aInsp}, substantially decreasing with increasing Q_{ECMO} (−0.15 per change of 1 L/min Q_{ECMO}) at baseline and PE conditions. In contrast, HPV led to increases in inspiratory VA coupling (fixed increase of 0.2 and additional increase of 0.08 per increase of 1 L/min Q_{ECMO}; Table 4, Figs. 2 and 5).

The expiratory EF followed VA $coupling_{Exp}$ and remained stable at approximately 66% of the ratio at baseline condition and zero Q_{ECMO}, with only minor variations seen during PE condition (Table 4). Inspiratory EF was lower at 59% for baseline conditions with zero Q_{ECMO} and followed VA $coupling_{Insp}$: EF_{Insp} was markedly reduced with increase in Q_{ECMO}, most accentuated at baseline and PE conditions (−4.2% per 1 L/min at baseline with an additional reduction of −1.2% per 1 L/min during PE, Table 4, Fig. 5). EF_{Insp} was less affected during HPV (2.7% less change per 1 L/min compared to baseline condition, Table 4). This resulted in linear relationship between EDV_{Exp} and ESV_{Exp} without additional relevant impact of Q_{ECMO} ($ESV_{Exp} = 0.40 \times EDV_{Exp} + 0.009 \times Q_{ECMO} \times EDV_{Exp} - 2.3$, $p < 0.001$, $r^2 = 0.85$). EDV_{Insp} shared a linear relationship with ESV_{Insp}, albeit with a higher coefficient which was additionally increased by Q_{ECMO} ($ESV_{Inspiratory} = 0.43 \times EDV_{Inspiratory} + 0.02 \times Q_{ECMO} \times EDV_{Inspiratory} + 0.2$, $p < 0.001$, $r^2 = 0.82$).

Stroke volume variation (SVV) was 28% at baseline and zero Q_{ECMO}. SVV increased by 13% per increase of 1 L/min of Q_{ECMO} at baseline. These changes were amplified during PE condition, with an additional change of 7% per increase of 1 L/min of Q_{ECMO}. During HPV, SVV was decreased compared to baseline (−18%, Table 4) and the variations associated with increasing Q_{ECMO} were also diminished (−9% per change of 1 L/min of Q_{ECMO}, Table 5, Fig. 3B).

Discussion

Main results

This post hoc study analyses the effects on the right ventricle and pulmonary vasculature of changing preload and afterload during VA ECMO weaning. Changing ECMO flow was used to model changing preload [21], such that increases in Q_{ECMO} reduced pulmonary blood flow, thereby unloading the right ventricle. These changes led to decreases in right and left atrial pressures, as blood volume was redistributed from the pulmonary to the systemic compartment [22, 23], and increased total blood flow (i.e., increased venous return) [21]. The decreasing left atrial pressures indicate that the left ventricle coped well with the afterload produced by the VA ECMO [2]. During Q_{ECMO} reductions, mean PA pressure increased as a consequence of increasing pulmonary blood flow [24], with a simultaneous decrease in input resistance (Z_0) and characteristic impedance (Z_c), attributable to improved distensibility and recruitment of the pulmonary vasculature [16, 25].

Effects of afterload increase

HPV and PE conditions acutely increased RV afterload. These changes were accompanied by small increases in RAP, indicating that the ventricles did not fail [26]. Rather, they operated below their stressed volumes [9, 26]. Both HPV and PE caused major increases in Z_0, Z_c

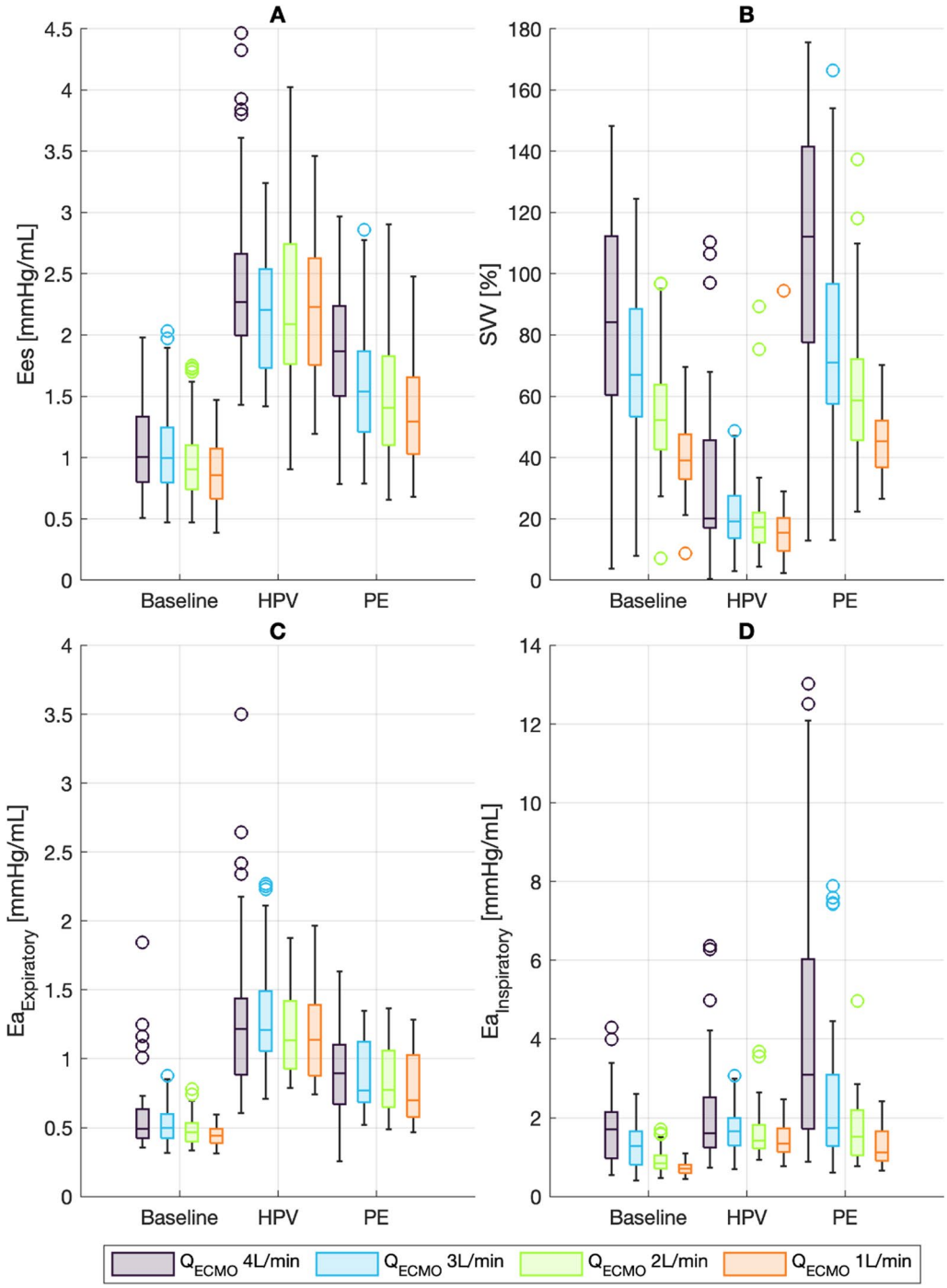

Fig. 3 Boxplots of right ventricular elastance (E_{es}) and pulmonary arterial elastance (E_a), presented by experimental condition and Q_{ECMO} (4, 3, 2, 1 L/min) as well as stroke volume variation (SVV). HPV: hypoxic pulmonary vasoconstriction. PE: pulmonary embolism. **A** Right ventricular elastance, calculated from the cardiac cycle with maximum stroke volume. **B** Stroke volume variation (SVV). **C** Pulmonary arterial elastance during expiration (E_{aExp}), calculated from the cardiac cycle with maximum stroke volume. **D** Pulmonary arterial elastance during inspiration (E_{aInsp}), calculated from the cardiac cycle with minimal stroke volume

remained unchanged compared to baseline as previously described [19, 20, 27].

During HPV and PE, the RV coped with acute afterload increases by increasing contractility (increased E_{es}) to maintain Q_{Lung} when Q_{ECMO} was decreased. This is in line with homeometric adaption (RV Anrep effect) [12, 17, 28]. Increased contractility from homeometric adaptation manifests as increased ventricular elastance (E_{es}),

Table 2 Estimates from linear mixed-effect models predicting right ventricular indices and ventricular–arterial coupling

	E_{es} [mmHg/mL]	E_{aInsp} [mmHg/mL]	E_{aExp} [mmHg/mL]
Intercept	0.83 [0.66 to 1.00]	0.37 [0.03 to 0.71]	0.39 [0.30 to 0.49]
HPV	1.36 [1.21 to 1.51]‡	0.89 [0.51 to 1.27]‡	0.75 [0.67 to 0.84]‡
PE	0.44 [0.29 to 0.59]‡	−0.35 [−0.73 to 0.02]	0.36 [0.27 to 0.44]‡
Q_{ECMO}	0.07 [0.03 to 0.10]‡	0.30 [0.21 to 0.39]‡	0.04 [0.02 to 0.06]‡
Q_{ECMO} × HPV	−0.03 [−0.09 to 0.02]	−0.12 [−0.26 to 0.02]	0.00 [−0.03 to 0.03]
Q_{ECMO} × PE	0.07 [0.01 to 0.12]*	0.65 [0.51 to 0.79]‡	0.01 [−0.03 to 0.04]
Adjusted r^2	0.69	0.45	0.69

Estimates from regression are shown with 95% CI. The intercept is the estimated value at 0 L/min Q_{ECMO} at baseline. HPV and PE estimates the change if the respective condition is present. Q_{ECMO} estimates the change per change of 1 L/min. Q_{ECMO} × HPV and Q_{ECMO} × PE estimates the additional change per change of 1 L/min of Q_{ECMO} during the respective condition. Inspiratory (Insp) and expiratory (exp) refer to the cardiac cycle with minimal and maximal stroke volumes, respectively. Q_{ECMO}: ECMO blood flow [L/min]. HPV: hypoxic pulmonary vasoconstriction. PE: pulmonary embolism. E_{es}: ventricular elastance. E_a: arterial elastance. *$p < 0.05$. ‡$p < 0.001$

to match the increases in afterload (i.e., arterial elastance, E_{aExp}). This mechanism restores RV–PA coupling to normal values (approximately 1.8 to 2.0; Figs. 2 and 5) [29] and establishes optimal energy transfer from the RV to the pulmonary vasculature [12]. Increases in ventricular elastance, in turn, lead to an increase in total (W_T) and oscillatory hydraulic work (W_{Osc}) with a constant W_T/W_{Osc} ratio.

Effects of the respiratory cycle

When preload was reduced by increasing Q_{ECMO}, the RV became more susceptible to afterload increases through the respiratory cycle, demonstrated by increases in E_{aInsp} during baseline and PE conditions. The resulting inspiratory RV–PA decoupling (Figs. 2 and 5) lead to reduced SV and enhanced SVV (Fig. 3B). This resulted from a combination of decreased filling and acute RV ejection inability. During states of normal preload (i.e., low Q_{ECMO}), the main cause of SVV was decreased filling—as demonstrated by only minor changes in RV–PA coupling. The additional relative respiratory cycle change in SV during conditions of low preload (i.e., high Q_{ECMO}) was a result of an acute RV inability to eject against the increased afterload (increased intrathoracic pressure). Previous studies explain inspiratory SV decrease predominantly as an effect of increased afterload [30, 31]. The time course of homeometric RV adaptation (Anrep effect) is unknown [12]. Respiratory cyclic changes of afterload occur too rapidly to allow for homeometric adaptation or "slow response" [32]. At low preload, the Starling mechanism (heterometric adaption), may not suffice to increase SV during inspiration, and does not restore ventricular–arterial coupling to preserve ejection fraction.

The increase in RV afterload was highest during HPV, as demonstrated by the highest input resistance (Z_0), mPAP, and E_{aExp}. Porcine pulmonary vasculature is highly reactive [20, 33]. Nevertheless, changes in inspiratory load at HPV condition were less pronounced compared to PE or baseline since only one lung was exposed to positive pressure ventilation.

Right ventricular behavior

Our study group has demonstrated that during VA ECMO, cardiac output can be estimated using gas exchange or modified thermodilution and that RV ejection fraction can be assessed from the exponential decay of the thermodilution signal [5, 6, 16, 34, 35]. In line with the findings of the present analysis, we could demonstrate that the EDV/ESV relationship was linear [16, 36]. The slope of EDV/ESV represents 1 – RVEF. We can

Table 3 Estimates from linear mixed-effect models predicting pulmonary arterial impedance and total and oscillatory hydraulic power

	Z_c [dyn × sec × cm^{-5}]	Z_0 [dyn × sec × cm^{-5}]	W_T [mW]	W_{Osc} [mW]
Intercept	132.8 [96.7 to 169.0]	267.7 [132.7 to 402.7]	1608.7 [1440.1 to 1777.3]	386.7 [320.4 to 453.0]
HPV	15.0 [−34.1 to 64.1]	609.7 [460.8 to 758.5]‡	888.2 [763.6 to 1012.8]‡	273.4 [225.8 to 321.0]‡
PE	40.6 [−8.2 to 89.4]	251.1 [103.2 to 399.1]‡	386.9 [263.1 to 510.7]‡	81.9 [34.6 to 129.2]‡
Q_{ECMO}	13.4 [1.7 to 25.1]*	123.6 [88.1 to 159.1]‡	−299.5 [−329.2 to −269.8]‡	−71.8 [−83.1 to −60.4]‡
Q_{ECMO} × HPV	−7.1 [−25.3 to 11.1]	−27.2 [−82.4 to 28.0]	−123.7 [−169.9 to −77.4]‡	−40.0 [−57.7 to −22.4]‡
Q_{ECMO} × PE	9.1 [−8.9 to 27.2]	0.7 [−54.1 to 55.5]	−80.8 [−126.7 to −35.0]‡	−16.5 [−34.0 to 1.1]
Adjusted r^2	0.10	0.38	0.73	0.62

Estimates from regression are shown with 95% CI. The intercept is the estimated value at 0 L/min Q_{ECMO} for baseline condition. HPV and PE estimates the change if the respective condition is present. Q_{ECMO} estimates the change per change of 1 L/min. Q_{ECMO} × HPV and Q_{ECMO} × PE estimates the additional change per change of 1 L/min of Q_{ECMO} during the respective condition. Q_{ECMO}: ECMO blood flow [L/min]. HPV: hypoxic pulmonary vasoconstriction. PE: pulmonary embolism. Z_c: characteristic pulmonary vascular impedance averaged over frequencies 2–15 Hz. Z_0: input resistance (impedance at 0 Hz). W_T: total hydraulic power. W_{Osc}: oscillatory hydraulic power. mW: milliwatt. *$p < 0.05$. ‡$p < 0.001$

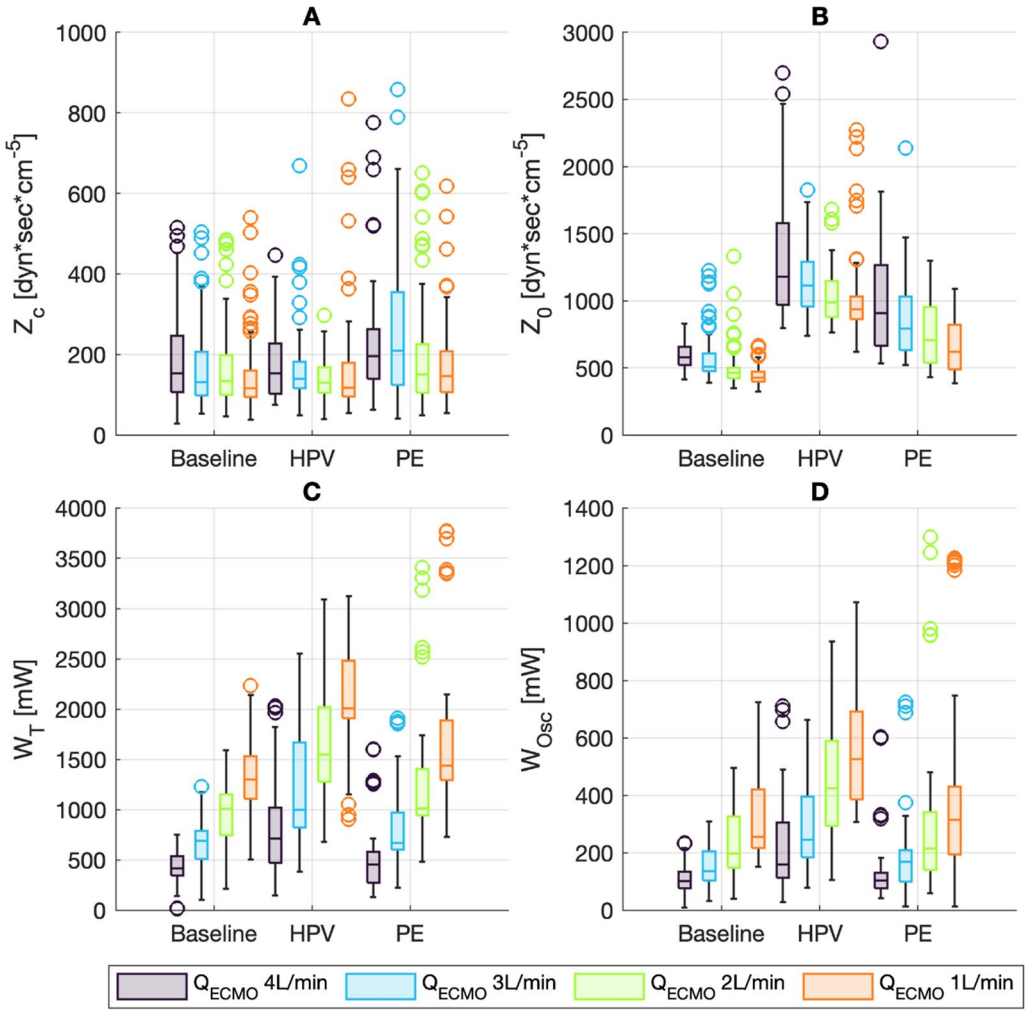

Fig. 4 Boxplots of pulmonary artery impedance and hydraulic work, presented by experimental condition and Q_{ECMO} (4, 3, 2, 1 L/min). HPV: hypoxic pulmonary vasoconstriction. PE: pulmonary embolism. **A** Characteristic pulmonary vascular impedance (Z_c), pressure and flow harmonics with amplitudes of < 1% of original signal excluded [19, 20]. **B** Input resistance (Z_0), defined as the impedance at 0 Hz. **C** Total hydraulic work (W_T). **D** Oscillatory hydraulic work (W_{Osc})

Table 4 Estimates from linear mixed-effect models predicting ventriculo-arterial coupling and ejection fraction

	VA coupling$_{insp}$	VA coupling$_{Exp}$	EF$_{Insp}$	EF$_{Exp}$
Intercept	1.4 [1.2 to 1.6]	2.1 [1.8 to 2.3]	59.4 [55.5 to 63.3]	66.0 [63.0 to 69.1]
HPV	0.2 [0.0 to 0.4]†	−0.1 [−0.3 to 0.1]	2.0 [−1.1 to 5.1]	−1.3 [−3.4 to 0.8]
PE	0.0 [−0.1 to 0.2]	−0.2 [−0.4 to 0.0]	−0.3 [−3.4 to 2.8]	−3.7 [−5.8 to −1.6]‡
Q_{ECMO}	−0.1 [−0.2 to −0.1]‡	0.0 [−0.0 to 0.1]	−4.2 [−4.9 to −3.4]‡	0.0 [−0.5 to 0.5]
Q_{ECMO} × HPV	0.1 [0.0 to 0.1]†	−0.0 [−0.1 to 0.1]	2.7 [1.6 to 3.9]‡	−0.1 [−0.9 to 0.6]
Q_{ECMO} × PE	−0.0 [−0.1 to 0.0]	0.0 [−0.0 to 0.1]	−1.2 [−2.4 to −0.1]*	0.8 [0.0 to 1.5]*
Adjusted r^2	0.49	0.45	0.54	0.44

Estimates from regression are shown with 95% CI. The intercept is the estimated value at 0 L/min Q_{ECMO} for baseline condition. HPV and PE estimates the change if the respective condition is present. Q_{ECMO} estimates the change per change of 1 L/min. Q_{ECMO} × HPV and Q_{ECMO} × PE estimates the additional change per change of 1 L/min of Q_{ECMO} during the respective condition. Q_{ECMO}: ECMO blood flow [L/min]. HPV: hypoxic pulmonary vasoconstriction. PE: pulmonary embolism. *$p < 0.05$. $^{\dagger}p < 0.01$. $^{\ddagger}p < 0.001$

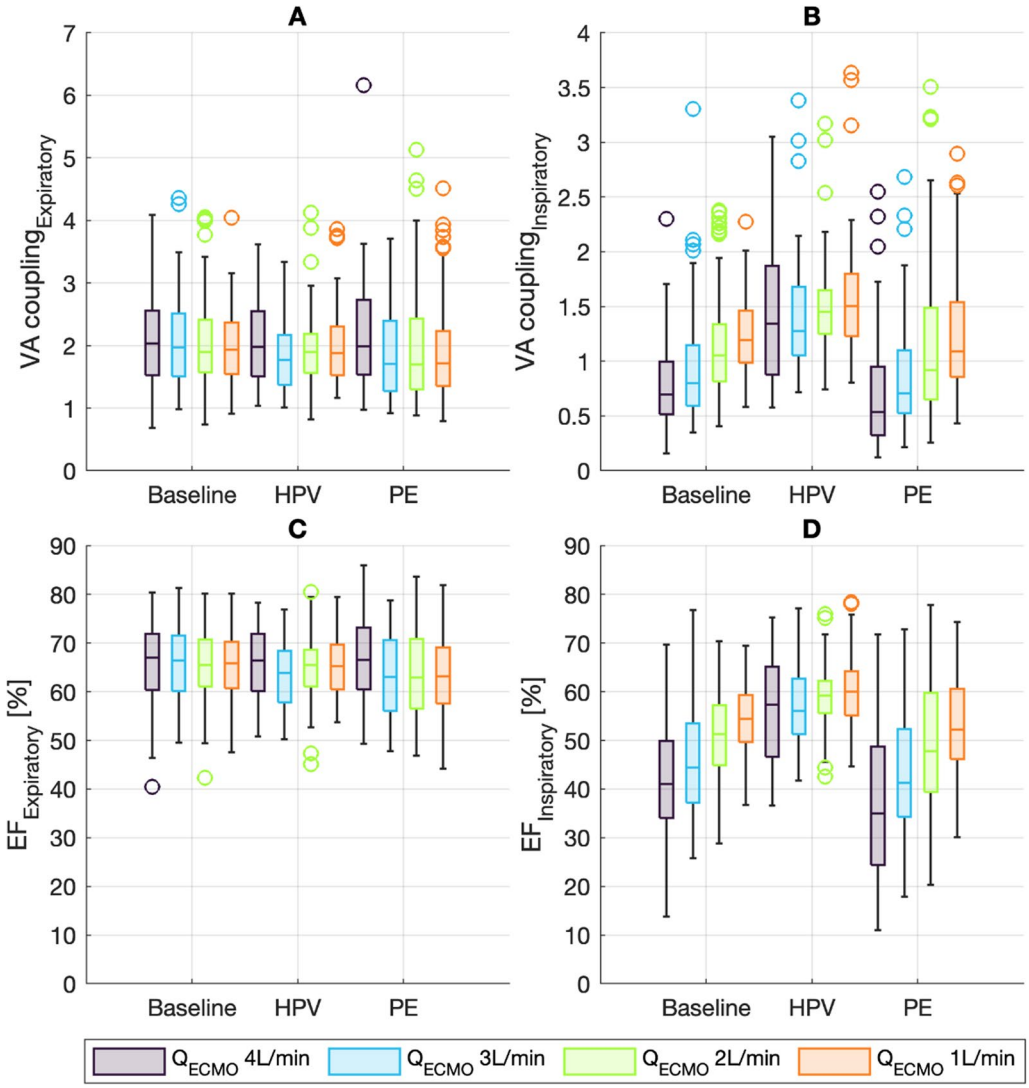

Fig. 5 Boxplots of ventricular–arterial coupling and ejection fraction, presented by experimental condition and Q_{ECMO} (4, 3, 2, 1 L/min). HPV: hypoxic pulmonary vasoconstriction. PE: pulmonary embolism. **A** Ventricular–arterial coupling during inspiration (VA coupling$_{Insp}$), calculated from the cardiac cycle with minimal stroke volume. **B** Ventricular–arterial coupling during expiration (VA coupling$_{Exp}$), calculated from the cardiac cycle with maximum stroke volume. **C** Ejection fraction during expiration (EF$_{Exp}$), calculated from the cardiac cycle with maximum stroke volume. **D** Ejection fraction during inspiration (EF$_{Insp}$), calculated from the cardiac cycle with minimal stroke volume

now extrapolate that the expiratory RVEF, remained constant during Q_{ECMO} variations. This suggests that the RV dilated to cope with increased preload [26], shifting the PV loop rightwards (Fig. 2). This dilation caused almost no increase in RAP. The RV end-diastolic PV relationship is flat at normal operating volumes [26]; increases in RAP by additional volume loading would therefore indicate RV failure [37]. During inspiration, the brisk combination of decreased preload and increased afterload prevented the ventricle from acute dilation and adaption, explaining the inspiratory decoupling and decrease in ejection fraction [30]. The PV loop is shifted left- and upwards (Fig. 2). While expiratory values remain constant and support the previous data on EDV/ESV relationship [16, 26, 36], we could demonstrate that acute inspiratory increases in afterload (e.g., E_{aInsp}) inhibit adequate RV ejection. This was most pronounced during states of low preload. Vieillard-Baron and colleagues had similar findings in echocardiographic studies: the respiratory cycle induced decreases in RV stroke volume, which were not associated with decreases in filling parameters and therefore interpreted as an afterload phenomenon [30, 31, 38]. It appears that although the RV can adapt to increases in afterload by increasing its contractility [28], the time

Table 5 Estimates from linear mixed-effect models predicting stroke volumes and end-diastolic volumes, including stroke volume variation (SVV)

	SV_{Min} [mL]	SV_{Max} [mL]	EDV_{Insp} [mL]	EDV_{Exp} [mL]	SVV [%]
Intercept	24 [22.3 to 25.6]	35 32.9 to 36.5]	43 [40.4 to 46.1]	53 [50.4 to 56.4]	28 [19.8 to 35.9]
HPV	−2.0 [−3.3 to −0.7]†	−9.5 [−11.0 to −8.0]‡	−6.5 [−8.75 to −4.2]‡	−14.1 [−16.5 to −11.6]‡	−17.6 [−24.7 to −10.56]‡
PE	−4.6 [−5.9 to −3.3]‡	−5.9 [−7.3 to −4.4]‡	−6.8 [−9.1 to −4.5]‡	−7.3 [−9.8 to −4.9]‡	−4.9 [−11.9 to 2.1]
Q_{ECMO}	−4.3 [−4.6 to −4.0]‡	−4.6 [−5.0 to −4.3]‡	−6.8 [−7.3 to −6.2]‡	−7.2 [−7.8 to −6.6]‡	13.3 [11.7 to 15]‡
Q_{ECMO} × HPV	1.7 [1.2 to 2.2]‡	2.0 [1.5 to 2.6]‡	2.6 [1.7 to 3.5]‡	3.1 [2.2 to 4.0]‡	−8.7 [−11.4 to −6.1]‡
Q_{ECMO} × PE	0.6 [0.1 to 1.1]*	0.7 [0.1 to 1.2]*	0.54 [−0.3 to 1.4]	0.7 [−0.2 to 1.6]	6.7 [4.1 to 9.3]‡
Adjusted r^2	0.70	0.66	0.65	0.64	0.70

Estimates from regression are shown with 95% CI. The intercept is the estimated value at 0 L/min Q_{ECMO} for baseline condition. HPV and PE estimates the change if the respective condition is present. Q_{ECMO} estimates the change per change of 1 L/min. Q_{ECMO} × HPV and Q_{ECMO} × PE estimates the additional change per change of 1 L/min of Q_{ECMO} during the respective condition. Q_{ECMO}: ECMO blood flow [L/min]. HPV: hypoxic pulmonary vasoconstriction. PE: pulmonary embolism. SV: stroke volume. SVV: stroke volume variation. EDV_{insp}: inspiratory end-diastolic volume. EDV_{exp}: expiratory end-diastolic volume *$p < 0.05$. †$p < 0.01$. ‡$p < 0.001$

available during the respiratory cycle is insufficient to allow for this adaptation [39]. The large variation in SV (Additional file 2: Fig. S1) may reflect RV–PA uncoupling rather than a pure preload dependency and is a result of preload decrease and simultaneous afterload increase [30, 40].

Clinical implications

Since the RV and PA are exposed to the same pressure at end-systole, ventricular–arterial coupling can be visualized as two intersecting lines at the end-systolic pressure (Fig. 2). This intersection divides the abscissa into end-systolic volume (ESV) on the side of E_{es}, and SV on the side of E_a. The RV and PA are exposed to the same pressure at end-systole. This end-systolic pressure provides a physiological and mathematical link between ventricular and arterial elastance, so that the ejection fraction can be determined by the E_{es}/E_a ratio or VA coupling [18]:

$$\frac{1}{EF} = \frac{E_a}{E_{es}} + 1 = \frac{1}{\text{VAcoupling}} + 1.$$

This is illustrated in Fig. 5 when comparing plots A&B with C&D [18]. From this equation, optimal coupling (ratio 1.5 to 2) will result in a RVEF of 60 to 67%.

When assessing right ventricular performance in a VA ECMO weaning trial, the EF, commonly accepted as a surrogate for contractility, depends on loading conditions and is an expression of RV–PA coupling [41]. It, therefore, seems reasonable to hypothesize that therapeutic measures improving contractility (for example, inotropes) and afterload (vasopressors or vasodilators, depending on the clinical context) should aim to improve coupling. In return, the right ventricular ejection fraction will increase. Pathological conditions leading to RV–PA decoupling will, therefore, inevitably lead to reduced ejection fraction, and with a clear understanding of coupling mechanisms, therapeutic options may be tailored to the underlying pathology. It is common to interpret a reduced ejection fraction as a consequence of low contractility. While this may be true in many cases, our results demonstrate that the ejection fraction is determined by contractility in combination with afterload and preload conditions. Lowering pulmonary vascular resistance (i.e., lowering pulmonary vascular elastance, E_a), optimizing volume status, or changing respiratory parameters and thereby decreasing right ventricular afterload may improve RV–PA coupling as efficiently as increasing contractility (E_{es}). We demonstrate that positive pressure ventilation in states of high afterload impacts right ventricular performance significantly, and positive pressure ventilation, therefore, may contribute significantly to disturbances in RV–PA coupling. If high pulmonary vascular resistance (i.e., high pulmonary vascular elastance, E_a) results from high left ventricular filling pressures, pharmacological or mechanical unloading of the left ventricular may optimize RV–PA coupling (and thereby RVEF) and interventions aimed directly at the right ventricle or pulmonary vasculature may not be necessary [2, 42]. It is therefore appealing to guide therapy and weaning from ECMO towards optimized coupling by directly influencing E_{es} (e.g., by increasing contractility) and E_a (by optimization of afterload and preload). Our analysis shows that right ventricular dilation is a physiological behavior of the right ventricle (i.e., heterometric adaption) to maintain RV–PA coupling. This should be considered in echocardiography guided weaning trials, where RV dilation is often seen as a weaning failure [43]. We demonstrate that dilation is a physiological adaptation if the RV operates below its stressed volume (i.e., at normal filling pressures). While we demonstrate the link between coupling and ejection fraction in the specific setting of VA ECMO, this physiological link, and the ensuing therapeutic targets (i.e., targeting E_a or E_{es}) could be applied to any hemodynamic assessment.

Limitations

We estimate higher RV ejection fractions in the current analysis than with our thermodilution approach. The reasons may be twofold: underestimation of the ejection fraction is common with thermodilution [44, 45]. We have shown that the exponential decay of thermodilution signals depends on the distance from the injection port [35]. Opposed to thermodilution studies where RVEF is estimated as a mean over multiple respiratory cycles, the elastance-based approach allows per beat calculation of EF during fractions of the respiratory cycle. Our findings are comparable to those of other groups [28].

We lack direct RV pressure signals. Instead, we rely on a modified single-beat method to estimate P_{isomax}, suggested by Pinsky [9]. Our estimations of E_a and E_{es} match published data from porcine PV loops [28]. We, therefore, judge the method to describe RV behavior reliably but conductance catheters are the gold standard to assess end-diastolic and end-systolic pressure–volume relationships [46].

The creation of HPV through main-stem intubation instead of using low levels of oxygen is a consequence of the retrospective nature of our study. In the protocol, we investigated the effects of shunt on a modified Fick principle. Therefore, both lungs were not evenly pressurized during HPV. Nevertheless, the diminished effect of lower intrathoracic pressure and one-lung ventilation on the reduction of RVEF and stroke volume variation highlights the impact of optimized ventilatory strategy in the setting of high right ventricular afterload.

Last, we lack transmural pressures in this experiment, which precludes us from fully differentiating the changes in stroke volume as a change of pre- or afterload [38, 46]. Additionally, our data did not allow for reconstruction of the end-diastolic PV relationship. The method of single-beat estimation from left ventricular EDPVR is not validated for RV use [47].

Conclusions

In conclusion, we have demonstrated that the RV, under support of VA ECMO, can increase its contractility in response to afterload changes to maintain adequate VA coupling. Abrupt additional increases in afterload by mechanical inspiration exhaust RV adaption ability. This effect was exacerbated in states of low preload. Assessment of RV function and RV–PA coupling using the here described approach is feasible with readily available bedside tools and provides an in-depth physiological in patients treated with VA ECMO. From this, future therapeutic concepts and weaning procedures may be built. We see RV–PA coupling as a key parameter for therapeutic optimization and guidance towards weaning success.

Abbreviations

VA ECMO	Veno-arterial extracorporeal membrane oxygenation
RV	Right ventricular
PA	Pulmonary artery
E_{es}	End-systolic elastance
E_a	Pulmonary arterial elastance
Q_{Lung}	Pulmonary blood flow
Q_{ECMO}	ECMO blood flow
RAP	Right atrial pressure
LAP	Left atrial pressure
mPAP	Mean pulmonary artery pressure
PE	Pulmonary embolism
HPV	Hypoxic pulmonary vasoconstriction
SV	Stroke volume
RVEF	Right ventricular ejection fraction
SVV	Stroke volume variation
Z_c	Characteristic impedance
Z_0	Input resistance
W_T	Total hydraulic power
W_{Osc}	Oscillatory hydraulic power
Ea_{Exp}	Expiratory arterial elastance
Ea_{Insp}	Inspiratory arterial elastance
ESV	End-systolic volume
EDV	End-diastolic volume
P_{isomax}	Right ventricular maximum isovolumetric pressure

Supplementary Information

The online version contains supplementary material available at https://doi.org/10.1186/s40560-024-00730-6.

Additional file 1. Visualization of full dataset.

Additional file 2: Figure S1. Boxplots of hemodynamic variables, presented by experimental condition and Q_{ECMO} (4, 3, 2, 1 L/min). HPV: Hypoxic pulmonary vasoconstriction. PE: Pulmonary embolism. **A**: Right atrial pressure. **B**: Left atrial pressure. **C**: pulmonary blood flow **D**: mean pulmonary arterial pressure. **E**: minimal stroke volume. **F**: maximal stroke volume. **G**: Heart rate. **H**: Mean systemic arterial blood pressure. **Figure S2**. Boxplots of peak vasopressor dose (Norepinephrine and epinephrine) for each condition. **A**: Peak norepinephrine dose. **B**: Peak epinephrine dose. **Table S1.** Protocol conditions.

Acknowledgements

Not applicable.

Author contributions

KFB and DB conceptualized the work. KFB performed data analysis and together with DB visually assessed data. KFB performed statistical analysis and drafted the first manuscript. PWM, LH and MM contributed with significant intellectual content, and revised the manuscript. All authors approved the final version of the manuscript.

Funding

The study was supported by grants from the "Stiftung für Forschung in Anästhesiologie und Intensivmedizin" (Bern, Switzerland; Nr 26/2018) awarded to Kaspar Bachmann and David Berger and by the "Fondation Johanna Dürmüller-Bol" (Muri bei Bern, Switzerland; Nr 481) awarded to Kaspar Bachmann.

Availability of data and materials

The dataset supporting the conclusions of this article is included within the article and its additional files.

Declarations

Ethics approval and consent to participate

The project was approved by the animal welfare committee of Bern (BE 111/18) and performed in accordance with the Swiss Ordinance on the Protection of Animals (TSchV 2008 455.1).

Consent for publication
Not applicable.

Competing interests
The Department of Intensive Care Medicine has, or has had in the past, research contracts with Abionic SA, AVA AG, CSEM SA, Cube Dx GmbH, Cyto Sorbents Europe GmbH, Edwards Lifesciences LLC, GE Healthcare, ImaCor Inc., MedImmune LLC, Orion Corporation, and Phagenesis Ltd. and research and development/consulting contracts with Edwards Lifesciences LLC, Nestec SA, and Wyss Zurich. The money was paid into a departmental fund; no author received any personal financial gain. The Department of Intensive Care Medicine received unrestricted educational grants from the following organizations for organizing a quarterly postgraduate educational symposium, the Berner Forum for Intensive Care (until 2015): Abbott AG, Anandic Medical Systems, Astellas, AstraZeneca, Bard Medica SA, Baxter, B | Braun, CSL Behring, Covidien, Fresenius Kabi, GSK, Lilly, Maquet, MSD, Novartis, Nycomed, Orion Pharma, Pfizer, and Pierre Fabre Pharma AG (formerly known as RobaPharm). The Department of Intensive Care Medicine has received unrestricted educational grants from the following organizations for organizing biannual postgraduate courses in the fields of critical care ultrasound, management of extracorporeal membrane oxygenation, and mechanical ventilation: Abbott AG, Anandic Medical Systems, Bard Medica SA., Bracco, Dräger Schweiz AG, Edwards Lifesciences AG, Fresenius Kabi (Schweiz) AG, Getinge Group Maquet AG, Hamilton Medical AG, Pierre Fabre Pharma AG (formerly known as RobaPharm), PanGas AG Healthcare, Pfizer AG, Orion Pharma, and Teleflex Medical GmbH.

Author details
[1]Department of Intensive Care Medicine, Inselspital, Bern University Hospital, University of Bern, Bern, Switzerland. [2]Department of Anesthesia, SV Hospital Group, Institute of Clinical Sciences at the Sahlgrenska Academy, University of Gothenburg, Gothenburg, Sweden. [3]Department of Cardiology, Inselspital, Bern University Hospital, University of Bern, Bern, Switzerland. [4]Medical Intensive Care Unit, University Hospital Zürich, University of Zürich, Zurich, Switzerland.

Received: 9 January 2024 Accepted: 14 April 2024
Published online: 11 May 2024

References

1. Chioncel O, Parissis J, Mebazaa A, et al. Epidemiology, pathophysiology and contemporary management of cardiogenic shock—a position statement from the Heart Failure Association of the European Society of Cardiology. Eur J Heart Fail. 2020;22(8):1315–41.
2. Bachmann KF, Berger D, Moller PW. Interactions between extracorporeal support and the cardiopulmonary system. Front Physiol. 2023;14:1231016.
3. Zeymer U, Freund A, Hochadel M, et al. Venoarterial extracorporeal membrane oxygenation in patients with infarct-related cardiogenic shock: an individual patient data meta-analysis of randomised trials. Lancet. 2023;402(10410):1338–46.
4. Burkhoff D, Sayer G, Doshi D, Uriel N. Hemodynamics of mechanical circulatory support. J Am Coll Cardiol. 2015;66(23):2663–74.
5. Berger DC, Zwicker L, Nettelbeck K, et al. Integral assessment of gas exchange during veno-arterial ECMO: accuracy and precision of a modified Fick principle in a porcine model. Am J Physiol Lung Cell Mol Physiol. 2023;324(2):L102–13.
6. Bachmann KF, Haenggi M, Jakob SM, Takala J, Gattinoni L, Berger D. Gas exchange calculation may estimate changes in pulmonary blood flow during veno-arterial extracorporeal membrane oxygenation in a porcine model. Am J Physiol Lung Cell Mol Physiol. 2020;318(6):L1211–21.
7. Koul B, Willen H, Sjoberg T, Wetterberg T, Kugelberg J, Steen S. Pulmonary sequelae of prolonged total venoarterial bypass: evaluation with a new experimental model. Ann Thorac Surg. 1991;51(5):794–9.
8. Millar JE, Fanning JP, McDonald CI, McAuley DF, Fraser JF. The inflammatory response to extracorporeal membrane oxygenation (ECMO): a review of the pathophysiology. Crit Care. 2016;20(1):387.
9. Pinsky MR. The right ventricle: interaction with the pulmonary circulation. Crit Care. 2016;20(1):266.
10. Rosch S, Kresoja KP, Besler C, et al. Characteristics of heart failure with preserved ejection fraction across the range of left ventricular ejection fraction. Circulation. 2022;146(7):506–18.
11. Ky B, French B, May Khan A, et al. Ventricular-arterial coupling, remodeling, and prognosis in chronic heart failure. J Am Coll Cardiol. 2013;62(13):1165–72.
12. Naeije R, Brimioulle S, Dewachter L. Biomechanics of the right ventricle in health and disease (2013 Grover Conference series). Pulm Circ. 2014;4(3):395–406.
13. Guarracino F, Ferro B, Morelli A, Bertini P, Baldassarri R, Pinsky MR. Ventriculoarterial decoupling in human septic shock. Crit Care. 2014;18(2):R80.
14. Trambaiolo P, Figliuzzi I, Salvati M, et al. Ventriculo-arterial coupling in the intensive cardiac care unit: a non-invasive prognostic parameter. Int J Cardiol. 2022;348:85–9.
15. Kim D, Park Y, Choi KH, et al. Prognostic implication of RV coupling to pulmonary circulation for successful weaning from extracorporeal membrane oxygenation. JACC Cardiovasc Imaging. 2021;14(8):1523–31.
16. Bachmann KF, Zwicker L, Nettelbeck K, et al. Assessment of right heart function during extracorporeal therapy by modified thermodilution in a porcine model. Anesthesiology. 2020;133(4):879–91.
17. Brimioulle S, Wauthy P, Ewalenko P, et al. Single-beat estimation of right ventricular end-systolic pressure-volume relationship. Am J Physiol Heart Circ Physiol. 2003;284(5):H1625-1630.
18. Mihaileanu S, Antohi EL. Revisiting the relationship between left ventricular ejection fraction and ventricular-arterial coupling. ESC Heart Fail. 2020;7(5):2214–22.
19. Maggiorini M, Brimioulle S, De Canniere D, Delcroix M, Naeije R. Effects of pulmonary embolism on pulmonary vascular impedance in dogs and minipigs. J Appl Physiol. 1998;84(3):815–21.
20. Maggiorini M, Brimioulle S, De Canniere D, Delcroix M, Wauthy P, Naeije R. Pulmonary vascular impedance response to hypoxia in dogs and minipigs: effects of inhaled nitric oxide. J Appl Physiol. 1995;79(4):1156–62.
21. Moller PW, Hana A, Heinisch PP, et al. The effects of vasoconstriction and volume expansion on veno-arterial ECMO flow. Shock. 2019;51(5):650–8.
22. Berger D, Moller PW, Weber A, et al. Effect of PEEP, blood volume, and inspiratory hold maneuvers on venous return. Am J Physiol Heart Circ Physiol. 2016;311(3):H794-806.
23. Moller PW, Winkler B, Hurni S, et al. Right atrial pressure and venous return during cardiopulmonary bypass. Am J Physiol Heart Circ Physiol. 2017;313(2):H408–20.
24. Naeije R. Pulmonary vascular resistance. A meaningless variable? Intensive Care Med. 2003;29(4):526–9.
25. Bshouty Z, Younes M. Distensibility and pressure-flow relationship of the pulmonary circulation. II. Multibranched model. J Appl Physiol. 1990;68(4):1514–27.
26. Pinsky MR, Desmet JM, Vincent JL. Effect of positive end-expiratory pressure on right ventricular function in humans. Am Rev Respir Dis. 1992;146(3):681–7.
27. Zuckerman BD, Orton EC, Latham LP, Barbiere CC, Stenmark KR, Reeves JT. Pulmonary vascular impedance and wave reflections in the hypoxic calf. J Appl Physiol. 1992;72(6):2118–27.
28. Ghuysen A, Lambermont B, Kolh P, et al. Alteration of right ventricular-pulmonary vascular coupling in a porcine model of progressive pressure overloading. Shock. 2008;29(2):197–204.
29. Tello K, Dalmer A, Axmann J, et al. Reserve of right ventricular-arterial coupling in the setting of chronic overload. Circ Heart Fail. 2019;12(1):e005512.
30. Valenti E, Moller PW, Takala J, Berger D. Collapsibility of caval vessels and right ventricular afterload: decoupling of stroke volume variation from preload during mechanical ventilation. J Appl Physiol. 2021;130(5):1562–72.
31. Vieillard-Baron A, Loubieres Y, Schmitt JM, Page B, Dubourg O, Jardin F. Cyclic changes in right ventricular output impedance during mechanical ventilation. J Appl Physiol. 1999;87(5):1644–50.
32. Cingolani HE, Perez NG, Cingolani OH, Ennis IL. The Anrep effect: 100 years later. Am J Physiol Heart Circ Physiol. 2013;304(2):H175-182.
33. Maggiorini M, Melot C, Gilbert E, Vermeulen F, Naeije R. Pulmonary vascular resistance in dogs and minipigs–effects of hypoxia and inhaled nitric oxide. Respir Physiol. 1998;111(2):213–22.
34. Bachmann KF, Vasireddy R, Heinisch PP, Jenni H, Vogt A, Berger D. Estimating cardiac output based on gas exchange during veno-arterial

extracorporeal membrane oxygenation in a simulation study using paediatric oxygenators. Sci Rep. 2021;11(1):11528.
35. Stanger EJ, Berger DC, Jenni H, Bachmann KF. Behaviour and stability of thermodilution signals in a closed extracorporeal circuit: a bench study. J Clin Monit Comput. 2023;37(4):1095–102.
36. Dhainaut JF, Pinsky MR, Nouria S, Slomka F, Brunet F. Right ventricular function in human sepsis: a thermodilution study. Chest. 1997;112(4):1043–9.
37. Magder S. Right atrial pressure in the critically ill: how to measure, what is the value, what are the limitations? Chest. 2017;151(4):908–16.
38. Berger D, Bloechlinger S, Takala J, Sinderby C, Brander L. Heart-lung interactions during neurally adjusted ventilatory assist. Crit Care. 2014;18(5):499.
39. Alviar CL, Miller PE, McAreavey D, et al. Positive pressure ventilation in the cardiac intensive care unit. J Am Coll Cardiol. 2018;72(13):1532–53.
40. Daudel F, Tuller D, Krahenbuhl S, Jakob SM, Takala J. Pulse pressure variation and volume responsiveness during acutely increased pulmonary artery pressure: an experimental study. Crit Care. 2010;14(3):R122.
41. Vanderpool RR, Pinsky MR, Naeije R, et al. RV-pulmonary arterial coupling predicts outcome in patients referred for pulmonary hypertension. Heart. 2015;101(1):37–43.
42. Ezad SM, Ryan M, Donker DW, et al. Unloading the left ventricle in venoarterial ECMO: in whom, when, and how? Circulation. 2023;147(16):1237–50.
43. Vieillard-Baron A, Naeije R, Haddad F, et al. Diagnostic workup, etiologies and management of acute right ventricle failure: a state-of-the-art paper. Intensive Care Med. 2018;44(6):774–90.
44. De Simone R, Wolf I, Mottl-Link S, et al. Intraoperative assessment of right ventricular volume and function. Eur J Cardiothorac Surg. 2005;27(6):988–93.
45. Santamore WP, Gefen N, Avramovich A, Berger P, Kashem A, Barnea O. Right atrial effects on right ventricular ejection fraction derived from thermodilution measurements. J Cardiothorac Vasc Anesth. 2007;21(5):644–9.
46. Berger D, Wigger O, de Marchi S, et al. The effects of positive end-expiratory pressure on cardiac function: a comparative echocardiography-conductance catheter study. Clin Res Cardiol. 2022;111(6):705–19.
47. Klotz S, Hay I, Dickstein ML, et al. Single-beat estimation of end-diastolic pressure-volume relationship: a novel method with potential for noninvasive application. Am J Physiol Heart Circ Physiol. 2006;291(1):H403-412.
48. Suga H, Sagawa K, Shoukas AA. Load independence of the instantaneous pressure-volume ratio of the canine left ventricle and effects of epinephrine and heart rate on the ratio. Circ Res. 1973;32(3):314–22.
49. Maughan WL, Shoukas AA, Sagawa K, Weisfeldt ML. Instantaneous pressure-volume relationship of the canine right ventricle. Circ Res. 1979;44(3):309–15.

Publisher's Note